

Article

Oxygen Sensing by the Hybrid Langmuir-Blodgett Films of Iridium(III) Complexes and Synthetic Saponite on the Basis of Energy Transfer

Hisako Sato ^{1,*}, Kenji Tamura ² and Akihiko Yamagishi ³

¹ Department of Chemistry, Graduate School of Science and Engineering, Ehime University, Matsuyama 790-8577, Japan

² National Institute of Materials Science, Tsukuba 305-0044, Japan; TAMURA.kenji@nims.go.jp

³ Department of Medicine, Toho University, Tokyo 143-8540, Japan; yamagishi@med.toho-u.ac.jp

* Correspondence: sato.hisako.my@ehime-u.ac.jp; Tel.: +81-89-927-9599

Received: 12 August 2017; Accepted: 28 September 2017; Published: 30 September 2017

Abstract: An ultra-thin hybrid film of amphiphilic iridium(III) complexes and synthetic saponite was manipulated by means of the modified Langmuir-Blodgett method. In the film deposited onto a quartz substrate, the external mixed molecular layer of amphiphilic iridium(III) complexes was reinforced by the inner layer of exfoliated synthetic saponite. As components of the molecular layer, two iridium(III) complexes were used: $[\text{Ir}(\text{dfppy})_2(\text{dc9bpy})]^+$ (dfppyH = 2-(4',6'-difluorophenyl)pyridine; dc9bpy = 4,4'-dinonyl-2,2'-bipyridine) (denoted as DFPPY) and $[\text{Ir}(\text{piq})_2(\text{dc9bpy})]^+$ (piqH = 1-phenyisoquinoline) denoted as PIQ). The emission spectra from the films changed from blue to red maxima with the decrease of a ratio of DFPPY/PIQ due to the energy transfer from excited DFPPY to PIQ. The intensity of red decreased with the increase of oxygen pressure through the quenching of excited iridium(III) complexes, promising a possibility as an oxygen-sensing film.

Keywords: iridium complexes; synthetic saponite; Langmuir-Blodgett method; phosphorescence; energy transfer

1. Introduction

Emission from an electronically-excited molecule is often used as a sensor output. It conveys various information, such as intensity, color, two-dimensional imaging, and so on. From a practical view-point, photo-sensing makes possible the detection from a remote position, requiring neither transparency nor homogeneity of samples. There have been a very large number of works accumulated to develop the molecules whose emission properties vary in response to the presence of other molecules or the variation of external circumstances. These are mostly concerned with molecules in a solution. Sensing is, however, of higher practical value when it takes the form of a thin film [1–4]. Sensing luminescent films are advantageous from the viewpoint of portability, tunable size, and recycling.

Among various techniques for preparing films, the Langmuir-Blodgett (LB) method provides an ultra-thin film with the high ratio of surface area to the total amount of a material [1,2,4]. A monomolecular layer of amphiphilic molecules is transferred from a water surface onto a solid substrate by a vertical or horizontal dipping method. When an appropriate luminescent molecule is used as an amphiphile, the deposited film is emissive enough to be detected with a conventional fluorometer. One problem of the method is, however, that an LB film is lacking in mechanical robustness, since molecules are arranged merely through the van der Waals interaction.

Recently, the hybridization of amphiphilic cations with clay minerals were attempted to prepare an LB film in order to overcome the disadvantage of fragileness [5–18]. Clay minerals are layered inorganic compounds. In case of smectite-type clays, they are readily exfoliated to sheets a few nanometer in

thickness (a so-called inorganic nanosheet). One layer consisted of two-dimensional networks of silica, alumina, or magnesia, or their fused multilayer sheets. A layer possesses a cation-exchange capacity on the order of 100 milliequivalents per g. A cationic species is adsorbed on the surface of the layer through the cation-exchange mechanism. In some cases, molecules on the surface are arranged regularly under the same orientation. Such regularity in adsorption might lead to unique photochemical or stereochemical aspects [19].

The clay LB method was first reported as the modification of the conventional LB method by two pioneering groups [6,7]. The basic principle is that a floating film of amphiphilic cationic molecules at an air-water interface is hybridized with clay particles (denoted as a clay nanosheet) exfoliated in an aqueous dispersion. The optimum conditions for preparing a clay hybrid film of high quality were studied extensively [8,9]. The surface morphology and layered structures of a deposited film were investigated by means of various spectroscopic methods [10]. The nanometer-thick films thus prepared were mechanically rigid in comparison to the LB films consisting of amphiphilic molecules alone.

Recently an emitting film was prepared by hybridizing a luminescent metal complex with synthetic saponite [16–18]. As an emitting element, cyclometalated iridium(III) complexes (denoted as Ir(III) complexes) were used due to their highly emitting properties in the visible region. A wide range of Ir(III) complexes have been explored in order to tune the emission wavelength [20,21]. The hybridization of an amphiphilic Ir(III) complex with various kinds of clay minerals was investigated [16,22–24]. In the case of synthetic saponite, for example, the emission was enhanced through the hybridization [25–29]. Similar enhancement was also realized by adsorbing Ir(III) complexes on a colloidal particle of synthetic saponite [30,31].

As a sensing device, the tuning of emitting light is an important factor to widen the wavelength range of monitoring light. One way to change the wavelength of the emitting light is to utilize the transfer of photon energy within a film. A red-shifted light is emitted as a result of energy transfer from an excited donor to an acceptor. For the purpose, two kinds of amphiphilic Ir(III) complexes with different emission maxima were employed. By changing the ratio of the donor to the acceptor in a film, the efficiency of the energy transfer was determined. Generally, red-emitting molecules are low in quantum yield in comparison to blue-emitting ones. The observed energy transfer would be utilized to enhance the emission intensity in the longer wavelength range. The sensing of oxygen was attempted by monitoring the red light from a hybrid film deposited onto a quartz substrate.

2. Materials and Methods

2.1. Materials

Cationic iridium(III) complexes, $[\text{Ir}(\text{dfppy})_2(\text{dc9bpy})]\text{ClO}_4$ ($\text{dfppyH} = 2\text{-}(2',4'\text{-difluorophenyl})$ pyridine, $\text{dc9bpy} = 4,4'\text{-dinonyl-2,2'}$ -bipyridine) (denoted by DFPPY) and $[\text{Ir}(\text{piq})_2(\text{dc9bpy})]\text{ClO}_4$ ($\text{piqH} = 1\text{-phenyisoquinoline}$) (denoted by PIQ), were synthesized according to the reported method [16]. The compounds were identified by mass spectra, $^1\text{H-NMR}$, and UV spectra, as reported previously [23]. Their molecular structures are shown in Chart 1.

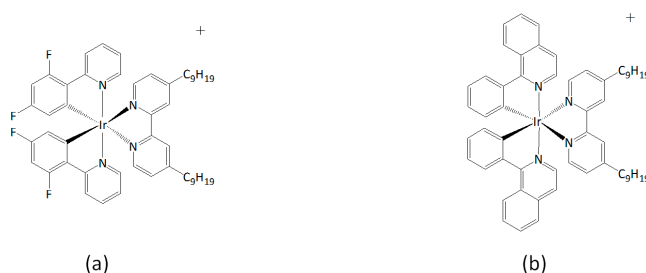


Chart 1. The structures of cations of the iridium(III) complexes used in this study: (a) $[\text{Ir}(\text{dfppy})_2(\text{dc9bpy})]^+$ (DFPPY) and (b) $[\text{Ir}(\text{piq})_2(\text{dc9bpy})]^+$ (PIQ).

Synthetic sodium saponite (Kunimine Ind. Co. Tokyo, Japan) with the elemental composition of $[(\text{Na}_{0.25}\text{Mg}_{0.07})(\text{Mg}_{2.98}\text{Al}_{0.01})(\text{Si}_{3.6}\text{Al}_{0.4})\text{O}_{10}(\text{OH})_2]$ (denoted by SAP) was used as a clay material. The cation-exchange capacity (CEC) of SAP, or the maximum amount of ion-exchangeable cations, is stated to be $0.80 \text{ meq}\cdot\text{g}^{-1}$.

2.2. Film Preparation and Characterization

A hybrid LB film of an Ir(III) complex and SAP was prepared as described below [23,24]. A trough with a surface area of $10.0 \text{ cm} \times 12.0 \text{ cm}$ (USI System, Fukuoka, Japan) was maintained at $20 \text{ }^\circ\text{C}$ by circulating water. For preparing a film of an Ir(III) complex hybridized with SAP (denoted as {Ir(III)/SAP}), 0.2 mL of chloroform solution containing a perchlorate salt of Ir(III) complex (ca. $5 \times 10^{-5} \text{ M}$) was spread over an aqueous dispersion of SAP ($10 \text{ mg}\cdot\text{L}^{-1}$). The ratio of DFPPY/PIQ in the spread solution was changed from 1 to 39. After 30 min, the surface of the trough was compressed at a rate of $10 \text{ cm}^2\cdot\text{min}^{-1}$ until the surface pressure reached 10 mNm^{-1} . Keeping the surface pressure at 10 mNm^{-1} for 30 min, the film was transferred onto a hydrophilic quartz plate ($1 \text{ cm} \times 2 \text{ cm}$) by the vertical deposition method at a dipping rate of $10 \text{ mm}\cdot\text{min}^{-1}$. The surface morphologies of hybrid films were investigated with an atomic force microscope (SPM-9600, Shimadzu Co. Ltd., Kyoto, Japan).

2.3. Electronic Absorption and Stationary Emission Measurements

UV-VIS electronic spectra were recorded with a U-2810 spectrophotometer (Hitachi, Hitachi, Japan). Emission spectra were measured with a fluorometer FP-6500 (JASCO, Tokyo, Japan) equipped with a Unispeks (UNISOKU, Oosaka, Japan) temperature-controlling cell holder. For the measurements of the emission spectra from a deposited film, the quartz substrate was placed at 45 degrees with respect to the incident light. The emitted light was detected at 90 degrees with respect to the incident light. The emission was measured in vacuum at room temperature.

2.4. Measurements of Emission Lifetime

The lifetime of emission was measured with a TSP-1000M-PL-ES (UNISOKU, Oosaka, Japan) at room temperature on a quartz plate modified with a hybrid film. The cell was evacuated to less than 0.1 kPa . The instrument was equipped with a pulse YAG laser at 355 nm . The emission decay curves were averaged for 130 transient signals. The width of a laser pulse was stated to be ca. 5 ns . The curves were simulated in terms of multi-exponential decays.

2.5. Sensing of Oxygen

The sensing of oxygen was performed by introducing oxygen gas into a cell containing a quartz plate modified with a hybrid film. The emission was measured at the maximum wavelength of the red-light emitter. For the measurements of the emission spectra, the quartz plate was placed at 45 degrees with respect to the incident light in the quartz cell. The emitted light was detected at 90 degrees with respect to the incident light. The emission was measured either in vacuum ($<0.1 \text{ kPa}$) or under oxygen atmosphere at room temperature.

3. Results and Discussion

3.1. Characterization of Deposited Hybrid Films

A deposited hybrid film containing a mixture of DFPPY and PIQ was prepared as described in the experimental section and is denoted as {DFPPY-PIQ/SAP}. Figure 1 shows the AFM image of {DFPPY-PIQ/SAP} at DFPPY/PIQ = 19. According to the image, the film consists of a flat ring-like domain with 400 nm in diameter and 5 nm in height. The domains would be formed by aggregation of SAP particles due to the adsorption of amphiphilic Ir(III) complexes. One particle of SAP was reported to be ca. 20 nm in diameter [32]. The external surface of each domain would be covered with the

layer of Ir(III) complexes and the inner part with the aggregated SAP particles. The same images were observed for DFPPY/PIQ = 1–39.

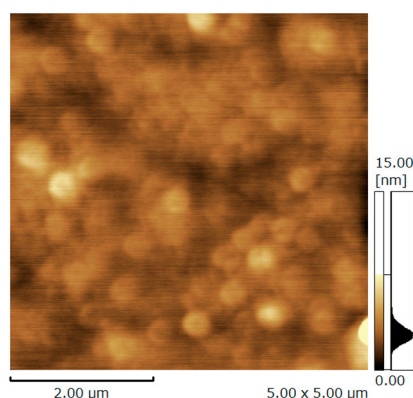


Figure 1. The AFM image of the hybrid film of {DFPPY-PIQ/SAP} deposited onto a quartz plate (DFPPY/PIQ = 19).

3.2. Stationary Measurements on Energy Transfer Processes

The deposited hybrid film of DFPPY or PIQ alone is denoted as {DFPPY/SAP} or {PIQ/SAP}, respectively. The emission spectra from these films under the excitation at 430 nm were reported in previous work [23,24]. The peak wavelength (λ_{\max}) of the emission spectrum was $\lambda_{\max} = 490$ nm for {DFPPY/SAP} and 590 nm for {PIQ/SAP}, respectively, reflecting the emission character of each Ir(III) complex incorporated in the film.

Figure 2 shows the emission spectra from {DFPPY-PIQ/SAP} at various DFPPY/PIQ ratios, when the films were irradiated at 430 nm in vacuum. Let the ratio of the emission intensity at $\lambda_{\max} = 490$ nm (mainly due to excited DFPPY) to that at $\lambda_{\max} = 590$ nm (mainly due to excited PIQ) be expressed by I_{490}/I_{590} . Apparently I_{490}/I_{590} depended remarkably on DFPPY/PIQ. In the following, the excited DFPPY and PIQ are denoted as DFPPY* and PIQ*, respectively. In case of DFPPY/PIQ = 1; for example, the spectra showed the low value of I_{490}/I_{590} ($\ll 1$). The results implied that the photon energy adsorbed by DFPPY was efficiently transferred to PIQ to produce PIQ*. The transfer of energy occurred through the Förster-type resonance mechanism. The occurrence of such energy transfer was guaranteed, since that the emission spectrum of DFPPY* overlapped appreciably the absorption spectrum of PIQ.

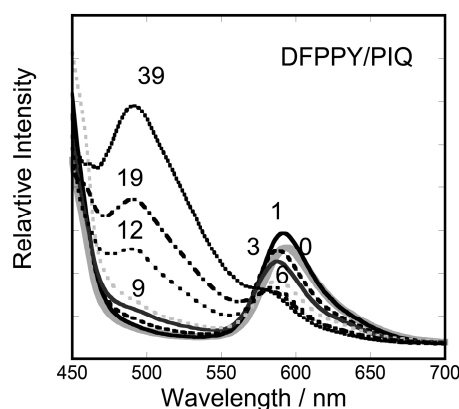


Figure 2. The change of the emission spectra from the hybrid films of {DFPPY-PIQ/SAP}: DFPPY/PIQ = 1, 3, 6, 9, 12, 19, and 39 in vacuum. Curve 0 (grey solid line) indicates the emission from {PIQ/SAP}.

3.3. Analyses of Stationary Emission Spectra on the Basis of the Förster-Type Mechanism

The results of the stationary emission spectra (Figure 2) were analyzed on the basis of the Förster-type energy transfer mechanism. According to the mechanism, the emission spectrum from {DFPPY-PIQ/SAP} is expressed by Equation (1) [27]:

$$F_{ET}(\nu) = (1 - \eta_{ET} - \phi_{dfpppy}) \times F_{dfpppy}^0(\nu) + \left(1 + \frac{1 - 10^{-A_{dfpppy}}}{1 - 10^{-A_{piq}}}\eta_{ET} - \phi_{piq}\right) \times F_{piq}^0(\nu) \quad (1)$$

in which $F_{ET}(\nu)$ is the emission spectrum at the wavelength (ν), $F_{dfpppy}^0(\nu)$ is the emission spectrum from {DFPPY/SAP} corrected for the concentration difference, $F_{piq}^0(\nu)$ is the modified emission spectrum from {PIQ/SAP} corrected for the concentration difference, η_{ET} is the energy transfer efficiency from the donor (DFPPY) to the acceptor (PIQ), ϕ_{dfpppy} is the quenching efficiency of the donor; and A_{dfpppy} (or A_{piq}) are the absorbance of the donor (or the acceptor) at 430 nm, respectively. The absorption spectra of the hybrid films were reported previously [23]. In the present cases, ϕ_{dfpppy} was taken to be zero. ϕ_{piq} represents the enhancement effect caused by hybridization with SAP. The best values of ϕ_{piq} are chosen from the range of -1 to -6.5 . The observed and calculated curves are compared as shown in Figure 3. The energy transfer efficiency (η_{ET}) is shown in Figure 4.

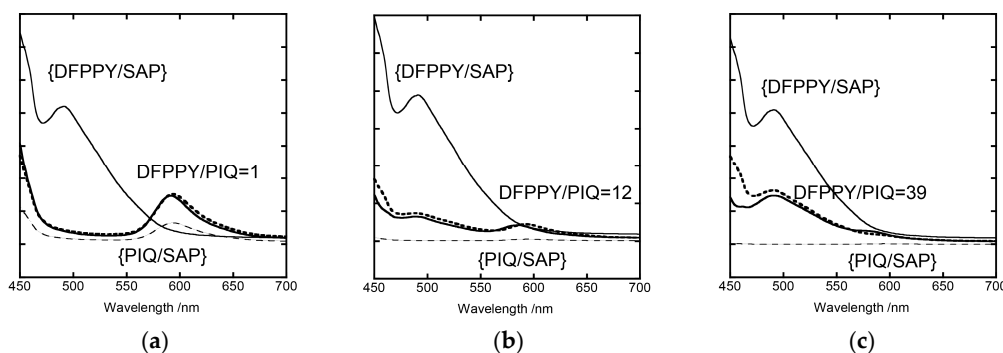


Figure 3. Examples comparing the experimental and calculated curves for the emission from the hybrid films of {DFPPY-PIQ/SAP} at DFPPY/PIQ = (a) 1, (b) 12, and (c) 39. Thin solid and broken lines show the {DFPPY/SAP} and {PIQ/SAP}, respectively. Solid lines are the experimental spectra and dotted lines are the calculated curves according to Equation (1), respectively.

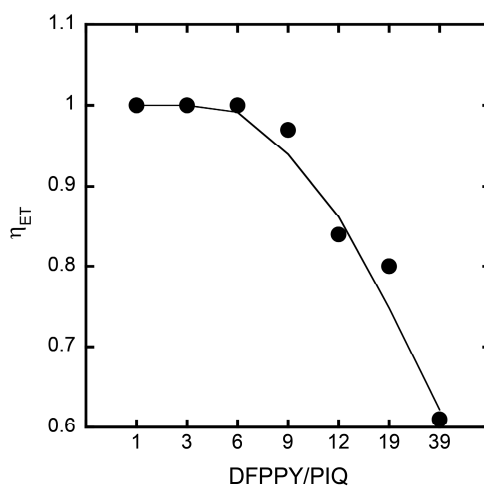


Figure 4. The dependence of the energy transfer efficiency (η_{ET}) within the hybrid film of {DFPPY-PIQ/SAP} on DFPPY/PIQ.

According to the analyses, the energy transfer efficiency was obtained to be as high as 60–100% for the range of DFPPY/PIQ = 1 to 39. The results implied that one PIQ molecule collected the photon energy migrating from several DFPPY* molecules. In other words, the harvesting of light energy took place in the present type of a hybrid film of a clay and Ir(III) complex.

3.4. Transient Measurements of the Energy Transfer Processes

The transient change of emission was monitored at 490 nm or 570 nm on {DFPPY-PIQ/SAP} at various values of DFPPY/PIQ in a vacuum. The films were irradiated by the light pulse at 355 nm. The time-course of emission at 490 nm or 570 nm represented, dominantly, the decay of DFPPY* or PIQ*, respectively. The examples of decay curves are shown in Figure 5. The decay curves were simulated by assuming the sum of two exponential components as below:

$$y = F_1 \exp(-t/\tau_1) + F_2 \exp(-t/\tau_2) \quad (2)$$

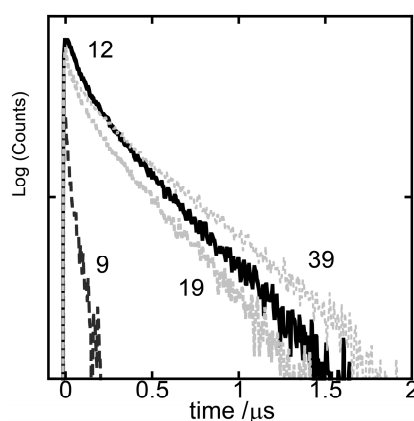


Figure 5. The time course of emission from the hybrid film of {DFPPY-PIQ/SAP} at DFPPY/PIQ = 9, 12, 19, and 39 at 490 nm.

According to Equation (2), two lifetimes were obtained for all films. The results are summarized in Table 1. The table also includes the pre-exponential factors, F_1 and F_2 , at 490 nm and 570 nm, respectively. The results indicated that the lifetime of DFPPY* decreased remarkably when the film contained both DFPPY and PIQ in comparison to the film containing DFPPY alone. Concomitantly, the lifetime of PIQ* increased in the presence of DFPPY in the same film. This implied that the energy transfer from DFPPY* to PIQ occurred efficiently within {DFPPY-PIQ/SAP}.

The origin for the presence of two relaxation paths for energy transfer might be sought in the heterogeneity of adsorption states. Both DFPPY and PIQ were adsorbed on the exfoliated layers of SAP due to electrostatic interaction. A part of the adsorbed molecules were located at the middle of a clay layer, while another part was located at the edge region. The former PIQ molecules would be more favorable for accepting photon energy from DFPPY molecules than the latter PIQ molecules. The situation was previously analysed by simulating the possible energy migration routes [23,24].

The rate of energy transfer is calculated according to Equation (3):

$$k_{ET} = 1/\tau - 1/\tau_D \quad (3)$$

where τ and τ_D denote the lifetimes of DFPPY in the presence and absence of PIQ, respectively. They were obtained from the decay curves of emission at 490 nm. The energy transfer efficiency, η_{ET} , is obtained according to Equation (4):

$$\eta_{ET} = k_{ET} / (k_{NT} + k_{ET}) \quad (4)$$

where k_{NT} is equal to $1/\tau_D$. Since the decay curve consisted of two components as stated above (Equation (2)), the analyses were performed independently for the fast and slow decay components. Figure 6 shows the dependence of η_{ET} on DFPPY/PIQ. The results indicated that η_{ET} took values as high as 50%–100% under the condition of DFPPY/PIQ = 1–9. This implied that the photon energy absorbed by several DFPPY molecules were captured efficiently to one PIQ molecule. In other words, the harvesting of light energy was also confirmed by the transient measurements. Although both static and transient measurements showed a similar trend, their results were not in complete agreement (e.g., compare the results between Figures 4 and 6). The observed discrepancy might be caused by the ambiguity in choosing parameters in estimating η_{ET} for both analyses.

Table 1. The lifetime of the emission from the hybrid films of {DFPPY-PIQ/SAP}.

DFPPY/PIQ	490 nm $\tau_1/\mu\text{s}$	490 nm $\tau_2/\mu\text{s}$	F ₁ #	F ₂ #
1	0.046	0.470	0.57	0.43
3	0.094	0.512	0.54	0.46
6	0.088	0.452	0.59	0.41
9	0.068	0.359	0.70	0.30
12	0.118	0.538	0.45	0.55
19	0.143	0.612	0.48	0.52
39	0.165	0.722	0.38	0.62
DFPPY/PIQ	570 nm $\tau_1/\mu\text{s}$	570 nm $\tau_2/\mu\text{s}$	F ₁ #	F ₂ #
1	0.263	1.33	0.46	0.54
3	0.209	1.41	0.41	0.59
6	0.203	1.17	0.49	0.51
9	0.167	1.41	0.48	0.52
12	0.178	0.77	0.43	0.57
19	0.194	0.813	0.43	0.57
39	0.199	0.89	0.37	0.63

(#) The relative amplitudes of the fast (F₁) and slow (F₂) components in the decay signals. c.f. The relaxation times were 0.176 μs (fast) and 0.945 μs (slow) at 490 nm and 0.177 μs (fast) and 0.826 μs (slow) at 570 nm for the hybrid film of {DFPPY/SAP}, respectively.

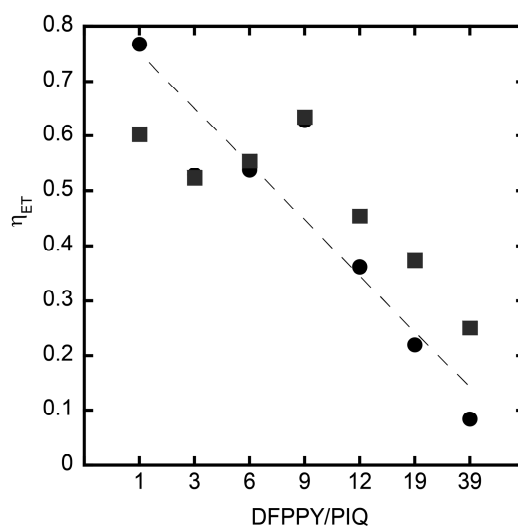


Figure 6. Dependence of energy transfer efficiency (η_{ET}) on DFPPY/PIQ for the hybrid film of {DFPPY-PIQ/SAP}. The solid circles and squares denote the fast and slow processes, respectively.

3.5. Oxygen Sensing by Hybrid Films Deposited onto a Quartz Plate

The effect of oxygen was studied on the emission from a clay-metal complex hybrid film deposited on a quartz substrate. Figure 7 shows the emission spectra, when a quartz substrate modified with {DFPPY-PIQ/SAP} at the ratio of DFPPY/PIQ = 1, 12, and 39, was irradiated at 430 nm, respectively. Measurements were performed under vacuum or oxygen atmosphere at room temperature. The emission profile of each film reflected the character of the composition of molecules. When an oxygen gas was introduced into the cell, the intensity of the emission decreased instantly (<10 s) due to the quenching of excited Ir(III) complexes by oxygen molecules. The intensity of the emission at the peak wavelength λ_{\max} due to excited PIQ was plotted as a function of partial pressure of an oxygen gas (P_{O_2}). The ratio of I_0/I was plotted against P_{O_2} (Stern-Volmer plots), in which I_0 or I was the emission intensity in vacuum or under oxygen atmosphere, respectively. As shown in Figure 8, the plots were nonlinear in the range of $P_{O_2} = 0$ –101.3 kPa for DFPPY/PIQ = 1–39 so that the curves were fitted on the basis of the following two-site model:

$$\frac{I_0}{I} = \left[\frac{f_1}{1+K_{sv1}C} + \frac{f_2}{1+K_{sv2}C} \right]^{-1}$$

$$f_1 + f_2 = 1 \quad (5)$$

$$K_{svav} = f_1 \times K_{sv1} + f_2 \times K_{sv2}$$

In Equation (5), K_{SV1} and K_{SV2} are two quenching parameters, and f_1 and f_2 their fractions, respectively. K_{svav} denotes the average value of the quenching constants, representing physically the initial slope of the plot near $P_{O_2} = 0$.

Table 2 shows the quenching parameters of K_{SV1} , K_{SV2} and K_{SVav} at various values of DFPPY/PIQ. The results demonstrated that the emission from the present hybrid films responded to the partial pressure of oxygen, indicating the possibility of oxygen sensing. When they were regarded as an oxygen sensor, an attention was paid to the lower pressure region of oxygen (<10 kPa). In this region, the plots were approximated by a straight line. The slope of the region was obtained as K_{SVav} in Table 2. According to the table, it was noted that the largest value of K_{SVav} was attained for the film at DFPPY/PIQ = 1. In this film, the quenching by oxygen took place mainly at DFPPY and the emission came from PIQ. In other words, DFPPY acted as an antenna for a target molecule and PIQ delivered sensed information. The highest sensitivity of sensing was accomplished through the concerting action of these two molecules. As an additional aspect, the emission from the hybrid films for DFPPY/PIQ = 1–9 was red since the energy transfer took place completely, while the emission from the films for DFPPY/PIQ = 12–39 was a mixture of red and blue lights due to the simultaneous emission both from DFPPY* and PIQ*. In this sense, the mixing of two kinds of Ir(III) complexes with different emitting characters might open a way of promoting the sensing ability and also tuning the monitoring light from the present type of molecular films.

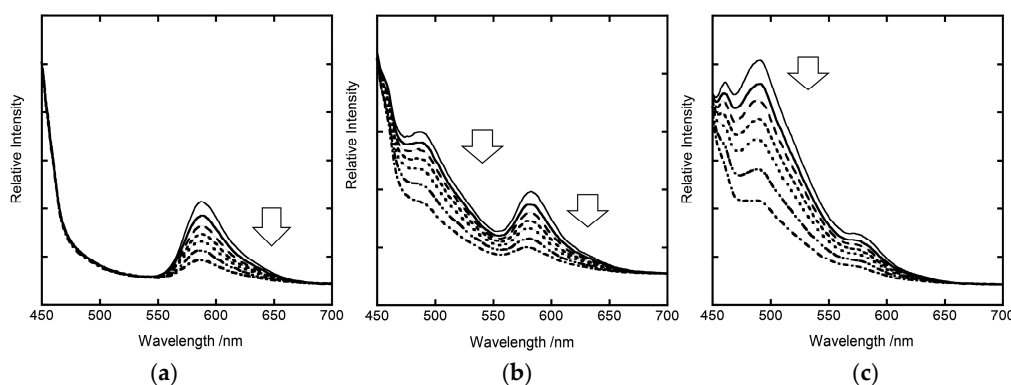


Figure 7. Oxygen sensing at DFPPY/PIQ = (a) 1, (b) 12, and (c) 39. The oxygen pressure is 0, 3, 6, 12, 25, 50, and 101.3 kPa.

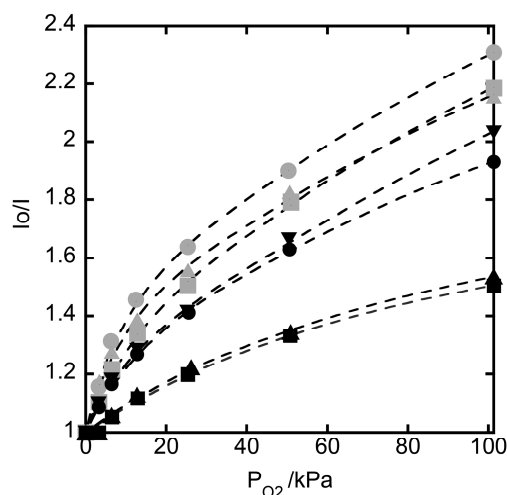


Figure 8. Stern-volmer plot of [DFPPY-PIQ]/SAP LB films: grey circle, grey square, grey triangle, filled black circle, filled black square, filled black triangle, and reverse filled triangle are DFPPY/PIQ = 1, 3, 6, 9, 12, 19, and 39, respectively. DFPPY/PIQ grey circle (1), grey square (3), grey triangle (6), filled black circle (9), filled black square (12), filled black triangle (19), and reverse filled black triangle (39).

Table 2. The Stern-Volmer parameters for quenching by oxygen (*).

DFPPY/PIQ	K_{sv1}	K_{sv2}	f_1	f_2	K_{svav}
1	0.0041	0.165	0.58	0.42	0.069
3	0.0042	0.095	0.60	0.40	0.038
6	0.0039	0.155	0.61	0.39	0.060
9	0.0030	0.077	0.62	0.38	0.029
12	0.0	0.018	0.48	0.51	0.009
19	0.0007	0.023	0.56	0.44	0.010
39	0.0049	0.115	0.70	0.30	0.034

(*) The parameters for DFPPY/PIQ = 1–9 or 12–39 were obtained by fitting the peak values or the peak areas of the emission spectra, respectively.

4. Conclusions

With the purpose of developing an emitting film for oxygen-sensing, the process of energy transfer was investigated by use of the mixed LB films containing two-types of iridium complexes as a donor and an acceptor. The films were reinforced by being hybridized with synthetic saponite. The efficiency of energy transfer was obtained as a function of the donor-to-acceptor ratio. The influence of oxygen gas on the emission at the longer wavelength (590 nm) led to the conclusion that the film increased its sensitivity toward oxygen by use of the energy transfer from the donor (blue-emitter) to the acceptor (red-emitter).

Acknowledgments: We thank Miwa Ochi (Ehime Univ.) for fabrication of the LB films and the measurement of the phosphorescence. This work has been financially supported by the MEXT KAKENHI Grant-Aid-for Scientific Research (B) JP26288039, JP17H03044, MEXT KAKENHI Grant-Aid-for Scientific Research (C) JP16K05762, and by the MEXT KAKENHI Grant-in-Aid for Exploratory Research JP16K15175.

Author Contributions: Hisako Sato conceived and designed the experiments; Hisako Sato and Kenji Tamura performed the experiments; Hisako Sato, Kenji Tamura and Akihiko Yamagishi analyzed the data; Kenji Tamura and Hisako Sato contributed reagents/materials/analysis tools; Hisako Sato and Akihiko Yamagishi wrote the paper.

Conflicts of Interest: The authors declare no conflict of interest.

References

1. Guan, W.; Zhou, W.; Lu, J.; Lu, C. Luminescent films for chemo- and biosensing. *Chem. Soc. Rev.* **2015**, *44*, 6981–7009. [[CrossRef](#)] [[PubMed](#)]
2. Neri, G. Thin 2D: The New Dimensionality in Gas Sensing. *Chemosensors* **2017**, *5*, 21. [[CrossRef](#)]
3. Sato, H.; Tamura, K.; Yamagishi, A. Luminescent Oxygen Gas Sensors Based on Nanometer-Thick Hybrid Films of Iridium Complexes and Clay Minerals. *Chemosensors* **2014**, *2*, 41–55. [[CrossRef](#)]
4. Sato, H.; Yamagishi, A. Application of the $\Delta\Lambda$ isomerism of Octahedral Metal Complexes as a Chiral Source in Photochemistry. *J. Photochem. Photobiol. C* **2007**, *8*, 67–84. [[CrossRef](#)]
5. Ras, R.H.; Umemura, Y.; Johnston, C.T.; Yamagishi, A.; Schoonheydt, R.A. Ultrathin hybrid films of clay minerals. *Phys. Chem. Chem. Phys.* **2007**, *9*, 918–932. [[CrossRef](#)] [[PubMed](#)]
6. Inukai, K.; Hotta, H.; Taniguchi, M.; Tomura, S.; Yamagishi, A. Formation of a clay monolayer at an air–water interface. *J. Chem. Soc. Chem. Commun.* **1994**, 959–960. [[CrossRef](#)]
7. Kotov, N.A.; Meldrum, F.C.; Fendler, J.H.; Tombácz, E.; Dékány, I. Spreading of Clay Organocomplexes on Aqueous Solutions: Construction of Langmuir-Blodgett Clay Organocomplex Multilayer Films. *Langmuir* **1994**, *10*, 3797–3804. [[CrossRef](#)]
8. Umemura, Y.; Yamagishi, A.; Schoonheydt, R.; Persoons, A.; de Schryver, F. Langmuir–Blodgett Films of a Clay Mineral and Ruthenium(II) Complexes with a Noncentrosymmetric Structure. *J. Am. Chem. Soc.* **2002**, *124*, 992–997. [[CrossRef](#)] [[PubMed](#)]
9. Umemura, Y.; Shinohara, E. Formation of Langmuir–Blodgett Films of a Clay and a Water-Soluble Alkylammonium Cation. *Langmuir* **2005**, *21*, 4520–4525. [[CrossRef](#)] [[PubMed](#)]
10. Shinohara, E.; Umemura, Y. Molecular orientation of Ru(II) complexes introduced in hybrid Langmuir-Scafer films of clay nanosheets and alkylammonium cations. *Thin Solid Films* **2013**, *542*, 373–379. [[CrossRef](#)]
11. Hirahara, M.; Umemura, Y. Fabrication of Three-Layer-Component Organoclay Hybrid Films with Reverse Deposition Orders by a Modified Langmuir–Schaefer Technique and Their Pyroelectric Currents Measured by a Noncontact Method. *Langmuir* **2016**, *31*, 8346–8353. [[CrossRef](#)] [[PubMed](#)]
12. Miguel, C.-L.; Coronado, E.; Ángel, L.-M.; Repetto, D.; Ito, T.; Konya, T.; Yamase, T.; Constable, E.C.; Housecroft, C.E.; Doyle, K.; et al. Dual-Emissive Photoluminescent Langmuir-Blodgett Films of Decatungstoeuropate and an Amphiphilic Iridium Complex. *Langmuir* **2010**, *26*, 1316–1324.
13. Huang, M.; He, S.; Liu, W.; Yao, Y.; Miao, S. Spectral Inspections on Molecular Configurations of Nile Blue Adsorbed on the Elementary Clay Sheets. *J. Phys. Chem. B* **2015**, *119*, 13302–13308. [[CrossRef](#)] [[PubMed](#)]
14. Debnath, P.; Chakraborty, S.; Deb, S.; Nath, J.; Bhattacharjee, D.; Hussain, S.A. Reversible Transition between Excimer and J-Aggregate of Indocarbocyanine Dye in Langmuir–Blodgett (LB) Films. *J. Phys. Chem. C* **2015**, *119*, 9429–9441. [[CrossRef](#)]
15. De Barros, A.; Ferreira, M.; José, C.; Constantino, L.; Bortoleto, J.R.R.; Ferreira, M. Synergy between Polyaniline and OMt Clay Mineral in Langmuir–Blodgett Films for the Simultaneous Detection of Traces of Metal Ions. *ACS Appl. Mater. Interfaces* **2015**, *7*, 6828–6834. [[CrossRef](#)] [[PubMed](#)]
16. Sato, H.; Tamura, K.; Ohara, K.; Nagaoka, S.; Yamagishi, A. Hybridization of clay minerals with the floating film of a cationic Ir(III) complex at an air–water interface. *New J. Chem.* **2011**, *35*, 394–399. [[CrossRef](#)]
17. Ohtani, Y.; Nishinaka, H.; Hoshino, S.; Shimada, T.; Takagi, S. Anisotropic photochemical energy transfer in clay/porphyrin system prepared by size-matching effect and Langmuir–Blodgett technique. *J. Photochem. Photobiol. A* **2015**, *313*, 15–18. [[CrossRef](#)]
18. Hussain, S.A.; Chakraborty, S.; Bhattacharjee, D.; Schoonheydt, R.A. Fluorescence Resonance Energy Transfer between organic dyes adsorbed onto nano-clay and Langmuir–Blodgett (LB) films. *Spectrochim. Acta Part A* **2010**, *75*, 664–670. [[CrossRef](#)] [[PubMed](#)]
19. Schoonheydt, R.A.; Umemura, Y. Clay Minerals as Natureal Nanosheets. In *Inorganic Nanosheets and Nanosheet-Based Materials*; Nakato, T., Kawamata, J., Takagi, S., Eds.; Springer: Tokyo, Japan, 2017; pp. 33–53, ISBN 978-4-431-56494-2.
20. Lowry, M.S.; Bernhard, S. Synthetically Tailored Excited States: Phosphorescent, Cyclometalated Iridium(III) Complexes and Their Applications. *Chem. Eur. J.* **2006**, *12*, 7970–7977. [[CrossRef](#)] [[PubMed](#)]
21. Martí, A.A. Metal complexes and time-resolved photoluminescence spectroscopy for sensing applications. *J. Photochem. Photobiol. A* **2015**, *307–308*, 35–47. [[CrossRef](#)]

22. Morimoto, K.; Nakae, T.; Ohara, K.; Tamura, K.; Nagaoka, S.; Sato, H. Dual emitting Langmuir–Blodgett films of cationic iridium complexes and montmorillonite clay for oxygen sensing. *New J. Chem.* **2012**, *36*, 2467–2471. [[CrossRef](#)]
23. Sato, H.; Tamura, K.; Ohara, K.; Nagaoka, S. Multi-emitting Properties of Hybrid Langmuir–Blodgett Films of Amphiphilic Iridium Complexes and the Exfoliated Nanosheets of Saponite Clay. *New J. Chem.* **2014**, *8*, 132–138. [[CrossRef](#)]
24. Sato, H.; Ochi, M.; Kato, M.; Tamura, K.; Yamagishi, A. Energy Transfer in Hybrid Langmuir–Blodgett Films of Iridium Complexes and Synthetic Saponite: Dependence of Transfer Efficiency on Interlayer Distance. *New J. Chem.* **2014**, *38*, 5715–5720. [[CrossRef](#)]
25. Tokieda, D.; Tsukamoto, T.; Ishida, Y.; Ichihara, H.; Shimda, T.; Takagi, S. Unique fluorescence behavior of dyes on the clay minerals surface: Surface Fixation Induced Emission (S-FIE). *J. Photochem. Photobiol. A* **2017**, *339*, 67–79. [[CrossRef](#)]
26. Eguchi, M.; Shimada, T.; Inoue, H.; Takagi, S. Kinetic analysis by laser flash photolysis of porphyrin molecules' orientation change at the surface of silicate nanosheet. *J. Phys. Chem. C* **2016**, *120*, 7428–7434. [[CrossRef](#)]
27. Ishida, Y.; Shimada, M.; Masui, D.; Tachibana, H.; Inoue, H.; Takagi, S. Efficient Excited Energy Transfer Reaction in Clay/Porphyrin Complex toward an Artificial Light-Harvesting System. *J. Am. Chem. Soc.* **2011**, *133*, 14280–14286. [[CrossRef](#)] [[PubMed](#)]
28. Morimoto, D.; Yoshida, H.; Sato, K.; Saito, K.; Yagi, M.; Takagi, S.; Yui, T. Light energy accumulation from pyrene derivative to tris(bipyridine)ruthenium on clay surface. *Langmuir* **2017**, *33*, 3680–3684. [[CrossRef](#)] [[PubMed](#)]
29. Sato, K.; Hagiwara, S.; Morimoto, D.; Saito, K.; Yagi, M.; Takagi, S.; Yui, T. Emission amplification of Ru(bpy)₃²⁺ via energy transfer from pyrene derivatives on synthesized clay. *J. Photochem. Photobiol. A* **2015**, *313*, 9–14. [[CrossRef](#)]
30. Sato, H.; Tamura, K.; Taniguchi, M.; Yamagishi, A. Efficient Energy Transfer of Cationic Iridium(III) Complexes on the Surface of a Colloidal Clay. *Appl. Clay Sci.* **2014**, *497–498*, 84–90. [[CrossRef](#)]
31. Tamura, K.; Yamagishi, A.; Kitazawa, T.; Sato, H. Harvesting of Light Energy by Iridium(III) Complexes on a Clay Surface. *Phys. Chem. Chem. Phys.* **2015**, *17*, 18288–18293. [[CrossRef](#)] [[PubMed](#)]
32. Takagi, S.; Shimada, T.; Ishida, Y.; Fujimura, T.; Masui, D.; Tachibana, H.; Eguchi, M.; Inoue, H. Size-Matching Effect on Inorganic Nanosheets: Control of Distance, Alignment, and Orientation of Molecular Adsorption as a Bottom-Up Methodology for Nanomaterials. *Langmuir* **2013**, *29*, 2108–2119. [[CrossRef](#)] [[PubMed](#)]



© 2017 by the authors. Licensee MDPI, Basel, Switzerland. This article is an open access article distributed under the terms and conditions of the Creative Commons Attribution (CC BY) license (<http://creativecommons.org/licenses/by/4.0/>).